Controlling and assessing the quality of aerosol jet printed features for large area and flexible electronics

2017 Flex. Print. Electron. 2 015004

(http://iopscience.iop.org/2058-8585/2/1/015004)

Flexible and Printed Electronics

OPEN ACCESS

RECEIVED
7 November 2016

REVISED
13 January 2017

ACCEPTED FOR PUBLICATION
20 January 2017

PUBLISHED
28 February 2017

PAPER

Controlling and assessing the quality of aerosol jet printed features for large area and flexible electronics

Michael Smith, Yeon Sik Choi, Chess Boughey and Sohini Kar-Narayan

Department of Materials Science and Metallurgy, University of Cambridge, CB3 0FS, United Kingdom

E-mail: sk568@cam.ac.uk

Keywords: aerosol jet printing, printed electronics, silver nanoparticle ink, flexible electronics

Supplementary material for this article is available online

Abstract

Aerosol jet printing (AJP) is a versatile technique suitable for large-area, fine-feature patterning of both rigid and flexible substrates with a variety of functional inks. In particular, AJP can tolerate ink viscosities between 1 and 1000 cP, with printing resolution of the order of 10 μm, thus making it attractive for flexible and printed electronics. This work investigates in detail significant aspects of ink-substrate combination and substrate temperature that are highly relevant to AJP. In order to do this, thin conducting silver lines are printed using AJP on both rigid (glass and silicon) as well as flexible (polyimide) substrates. The correlation between the various deposition parameters and the 'quality' of the printed lines are evaluated, through measurements of electrical conductivity under different experimental conditions. Based on our findings, a framework is proposed through which the morphology of AJP lines can be controlled and assessed for applications in large area and flexible electronic devices.

1. Introduction

Additive manufacturing promises to be the future of consumer device production; the ability to deposit material only where it is needed increases the rate of manufacture, reduces the amount of waste and permits innovative device design [1, 2]. Patterning large area and flexible electronic circuits is of particular interest [3], especially given the advance of the 'Internet of Things' and the forecast of a dramatic increase in the number of connected and wearable devices. In this respect, inkjet printing (IJP) is perhaps one of the most well-established additive manufacturing techniques, with a large amount of research and a number of commercially available printers and metallic nanoparticle inks [4].

In comparison, aerosol jet printing (AJP) is a relatively new additive manufacturing technique which offers a more versatile alternative to IJP, especially when it comes to the selection of suitable inks for deposition. Unlike in IJP where droplets of ink are individually placed on the substrate and coalesce to form a continuous layer, AJP involves creating a fine mist, or 'aerosol', of ink and using a carrier gas to jet this aerosol towards a substrate. Seifert *et al* conducted a comprehensive comparison of AJP and IJP in the context of depositing silver nanoparticle inks, highlighting the key differences and benefits of each technique [5]. One of the most significant advantages of AJP indeed comes when considering the variety of materials that can be deposited beyond metallic nanoparticle inks.

While IJP is limited to a narrow range of ink viscosities, typically between 10 and 40 cP [6], AJP can tolerate viscosities between 1 and 1000 cP, allowing materials such as polymers [7, 8], biological material [9, 10], carbon nanotubes [11] and other semiconducting materials [12] to be deposited over relatively large areas (of the order of tens of centimetres) with printing resolution of the order of 10 μm. This is especially important if additive manufacturing is to develop into a viable production route for entire devices, whereby active components such as sensors, resistors and capacitors can also be printed alongside conducting metal tracks. In this respect, understanding the characteristics of the AJP technique is important to further the progress in this field. This work investigates the effect of various AJP deposition

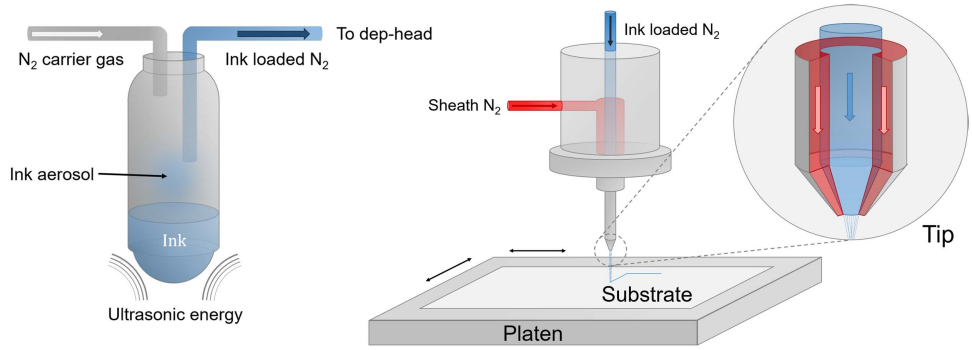

Figure 1. A schematic of the aerosol jet process using an ultrasonic atomiser.

parameters on the quality of lines printed using a silver nanoparticle ink.

A schematic of the aerosol jet process is shown in figure 1. In AJP, an atomiser is used to create an aerosol of ink droplets typically 1–5 μm in diameter. For this study, an ultrasonic atomiser has been used, although other atomisation methods are possible. This aerosol is entrained in a nitrogen carrier gas and fed towards the deposition head (dep-head). Within the dep-head, a second gas flow—the 'sheath' flow—is introduced and surrounds the atomiser gas flow. These gases flow co-axially through the dep-head and out of the tip, the opening of which is between 100 and 300 μm in diameter. The focussing effect of the sheath gas means that features down to 10 μm can be printed under appropriate conditions. By mounting a substrate beneath the tip on an automated platen, wide area deposition of these fine features is possible. For the printer used in this study, platen motion is controlled using x–y linear stepper motors with micron resolution, although in principle the process can be used with any positioning system. Typically, platen motion is not the limiting factor for print resolution.

In this setup, the rate of each gas flow can be varied independently, allowing for the dynamics of the aerosol jet to be controlled with reasonable precision. Many other aspects of the deposition process can also be varied, such as tip diameter, tip-substrate separation (tip height), substrate temperature, ink temperature and print speed. Goth *et al* presented some initial investigations on the sensitivity of the process to some of these parameters [13]. Mahajan *et al* subsequently carried out a more systematic study into the influence of these parameters on the morphology and electrical properties of silver lines printed onto silicon [14]. Specifically, they identified the 'focus ratio'—the ratio of the sheath gas flow rate to the atomiser gas flow rate—as a key quantity in controlling the aspect ratio of the line.

This same parameter was also identified by Binder *et al* while developing an analytical model to predict the width of the printed line and investigate a phenomenon within AJP known as 'overspray', where small droplets of ink within the aerosol jet deviate from the centre of the gas flow [15]. Impinging on the substrate a distance away from the centre, the width of the line increases as the edges become ill-defined and therefore 'fuzzy'. This has significant implications on the spatial resolution of the technique, forcing an increase in line separation, though the exact causes of overspray are not yet fully understood.

In this work, in addition to the effect of sheath flow rate and atomiser flow rate, we investigate the influence of substrate temperature on the morphology of lines printed using a silver nanoparticle (Ag NP) ink, and we show that this is an important parameter in the AJP process. Our studies are performed on three different substrate materials (both rigid and flexible) to determine how the deposition characteristics transfer between substrates. This was briefly eluded to by Folgar *et al* during their formulation of a ceramic ink for AJP, but is investigated here for Ag NP ink in detail [16].

Importantly, detailed studies of the control and analysis of the quality of AJP printed lines are shown here for flexible substrates. AJP is a promising technology for flexible electronics; Mahajan *et al* have demonstrated that AJP can be used as part of an insertion, curing and delamination method to produce flexible conducting structures [17]. It has also been shown that additions such as graphene can be used to improve the flexibility of AJP Ag NP inks [18]. Here, we introduce a method for assessing the flexibility and integrity of conducting structures printed onto flexible substrates. More generally, a method of characterising the phenomenon of overspray is presented here for the first time, as well as an investigation into system drift in AJP, whereby the print output changes over time. Finally, the process of arriving at an acceptable set of deposition parameters for a given application is discussed.

2. Methods

2.1. Printing methods

The print system used in this work was an AJ200 from Optomec (Optomec Inc., New Mexico, USA) equipped

with an ultrasonic atomiser (UA Max—Optomec). This device creates an aerosol by exciting the ink with ultrasonic pressure waves. The atomiser current was set to maximum (0.6 mA) for each print. A silver nanoparticle ink was used for this investigation (Prelect TPS 50 G2—Clariant), diluted 1:3 by volume with de-ionised water (ink:water). For each printing run 1.2 ml of the ink:water solution was used. The ink temperature was held constant at 20 °C using a water bath during printing, and between sessions the ink was kept refrigerated. A tip diameter of 150 μm and tip height of 3 mm were used throughout. Other parameters that were varied as part of the investigation included sheath flow rate (20 → 160 sccm), atomiser flow rate (20 → 32 sccm), print speed (0.1 → 10 mm s^{-1}) and substrate temperature (20 → 100 °C). Gas flow rates are quoted in standard cubic centimetres per minute (sccm).

A variety of substrates including silicon wafer (with native oxide), glass and polyimide (5 mils, DuPont) were used. All substrates were washed in acetone and dried with nitrogen gas prior to printing. No surface modification was carried out and a single pass was used for all prints. Curing was carried out immediately after printing using an oven (HeraTherm—Thermo Scientific). Unless otherwise stated, curing was carried out at 200 °C for 1 h. A Dektak profilometer (Veeco) was used to measure the resulting line profiles, with five profiles being recorded per sample. The area for each profile was determined by numerically evaluating the area underneath the peak profile using proprietary code written in MATLAB (R2016a, Mathworks), from which an average value and standard error was obtained.

Similar to the procedure followed by Binder *et al* [15], two methods were used here to measure the line width. In the aforementioned study, these criteria were used to provide upper and lower bounds of line width to verify an analytical model. Here, they were compared directly to quantify the quality of a printed line. The first method used micrographs of the lines obtained with a desktop scanning electron microscope (SEM) (Hitachi TM3030Plus). The edge of what was deemed to be overspray was subjectively selected, and from these edges an effective line width (w_{eff}) was measured. This was repeated for several images of each line and an average taken. The second width criterion was taken as the full width at half maximum (FWHM) of the peak profile obtained using the profilometer. This was evaluated using the peak find function in MATLAB. In all cases the error is presented as the standard error in the mean. An illustration of the integrated area, FWHM and SEM width are shown in figure S1 within the supplementary information.

The ratio of the two widths, given by

$$\text{Width Ratio} = \frac{w_{\mathrm{eff}}}{\mathrm{FWHM}} \qquad (1)$$

was used to assess the quality of the printed line. If w_{eff} was found to be significantly larger than the FWHM, overspray was identified as an issue since a large proportion of material was not contributing the current carrying capacity of the line. That is, the width of the line was increased but with no benefit to conductivity. High quality lines would have a width ratio close to unity.

For the investigation into system drift, the printer was run continuously for 60 min using the following print parameters; sheath 60 sccm, atomiser 28 sccm, substrate temperature 60 °C and print speed 1 mm s^{-1}. For the investigation into substrate temperature, samples were deliberately printed out of sequence to mitigate the effects of the system drift. Furthermore, the print time was kept to a minimum to prevent a significant variation. At each selected platen temperature, lines were printed on each substrate material in quick succession and the order of printing (i.e. glass → polyimide → silicon) was randomised for each substrate temperature. Separate substrates were used for each temperature, these were removed immediately after printing before the next set of substrates were mounted and left for 5 min to equilibrate once the platen had reached the new temperature.

2.2. Electrical characterisation methods

The patterns used for electrical characterisation were designed to allow a 4-point conductivity measurement over a path length of 15 mm—schematics of the toolpaths used can be found in the supplementary information, figure S2. This was carried out under ambient conditions using a lock-in amplifier (Signal Recovery–7265 DSP). The sample was connected in series with a current limiting resistor, roughly 50x the resistance of the sample. An oscillating voltage of 5 V at 1000 Hz was applied to the circuit, and the potential across the sample measured with phase sensitive detection using the internal reference oscillator of the amplifier. Measurements of electrical conductivity provided a useful means to determine the quality of the AJP printed lines. These measurements also provided insight into the line quality and integrity on flexible substrates, which were subjected to controlled bending while electrical conductivity was monitored.

In this work, polyimide was used as a flexible substrate and a modified pattern was designed to allow the resistance of the line to be assessed *in situ* as the samples were deformed to a constant curvature. This was achieved by bending the substrate around cylinders of various known diameters. Using the electrical transport measurement method described above, the resistance was measured while the substrate was flat (R_0) and then again once the sample was deformed (R), thus allowing for the strained and unstrained resistances to be compared. These pairs of measurements were carried out for each value of curvature until sample failure. Failure was determined when fewer than 3 samples were conducting for a given curvature. A schematic of this flex-testing procedure is shown in figure S4.

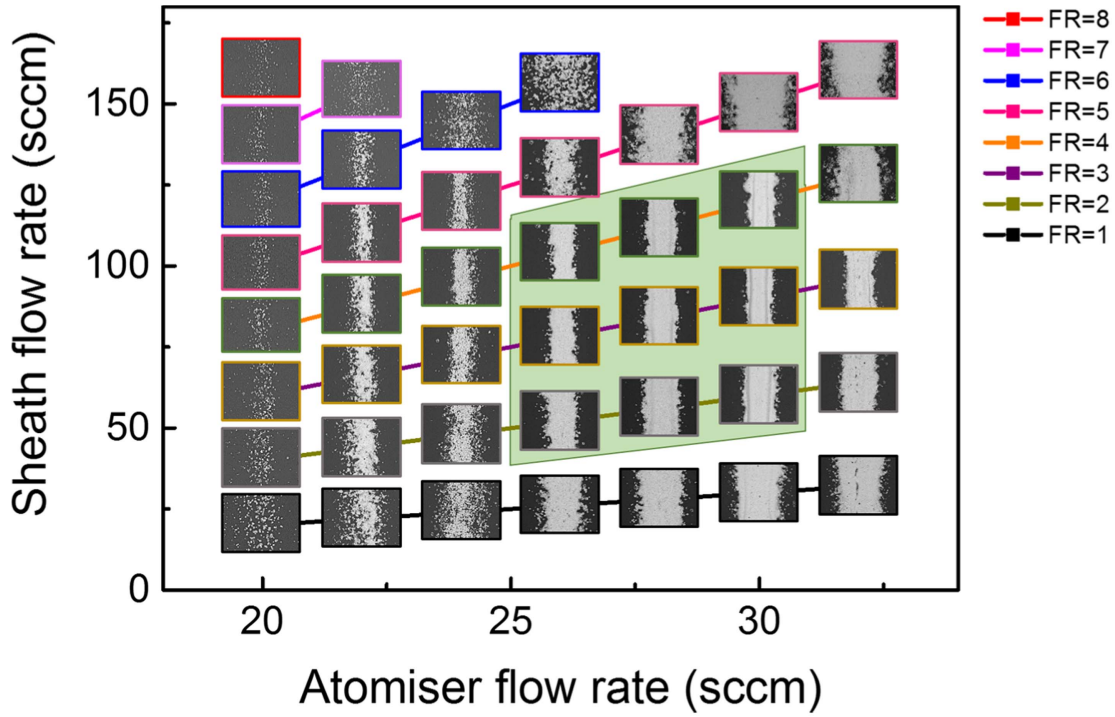

Figure 2. The influence of two gas flows on line morphology. Lines printed at the same focus ratio (FR = sheath flow rate/atomiser flow rate) are grouped together. A clear operability window (highlighted green) can be seen for atomiser flow rates between 26 and 30 sccm, with focus ratios between 2 and 4.

3. Results

The influence of the two gas flow rates on the line morphology is demonstrated in figure 2. These lines were printed onto silicon at a platen temperature of 60 °C. Following the example of Mahajan *et al* [14], the focus ratio (FR = sheath flow rate/atomiser flow rate) of each deposition is also highlighted. It was found that a minimum atomiser flow rate of around 25 sccm had to be reached in order to produce a continuous line. For each value of atomiser flow rate, the deposition could be seen to pass through an operational window as the focus ratio was increased. Using a low focus ratio produced lines that were broad and ill-defined. Increasing the focus ratio improved the deposition, yielding lines with more distinct edges. Increasing the ratio further resulted in lines that were once again poorly-defined. In this way, an optimal window for deposition could be determined. Figure 2 demonstrates that for this particular system (i.e. the combination of printer, ink, substrate, temperature and print speed), acceptable deposition occurs for atomiser flow rates of between 26 and 30 sccm with focus ratios between 2 and 4.

Following these results, deposition parameters listed in table 1 were used for the subsequent investigations. SEM images of lines printed onto silicon, glass and polyimide using these parameters at various substrate temperatures are shown in figure 3.

The morphology of the lines printed onto all three substrates at 20 °C was reasonably similar. Differences between the substrates became apparent as the substrate temperature was increased. Cracks close to the line edge can be seen in the sample printed on glass at higher temperatures. Temperature induced overspray was found on all substrates, however silicon appeared to be the most significantly affected.

Table 1. Deposition parameters determined as a result of the initial investigation.

Parameter	Value (units)
Sheath flow rate	60 sccm
Atomiser flow rate	28 sccm
Print speed	1 mm s^{-1}

The influence of substrate temperature on both line width criteria is shown in figure 4(a). There is a general trend of decreasing line width with increasing substrate temperature, however in all cases the lines printed at 20 °C were found to be narrower than those printed at 40 °C. For silicon, this trend also extended to 60 °C. A slight increase in w_{eff} was observed on polyimide and silicon substrates for the highest substrate temperatures as overspray became more prominent. Line widths were found to be comparable between substrates for a given temperature. The results shown in the plots in figure 4(a) are in good qualitative agreement with the observations of the SEM images shown in figure 3.

The calculated width ratio is shown in figure 4(b). This decreased with increasing substrate temperature

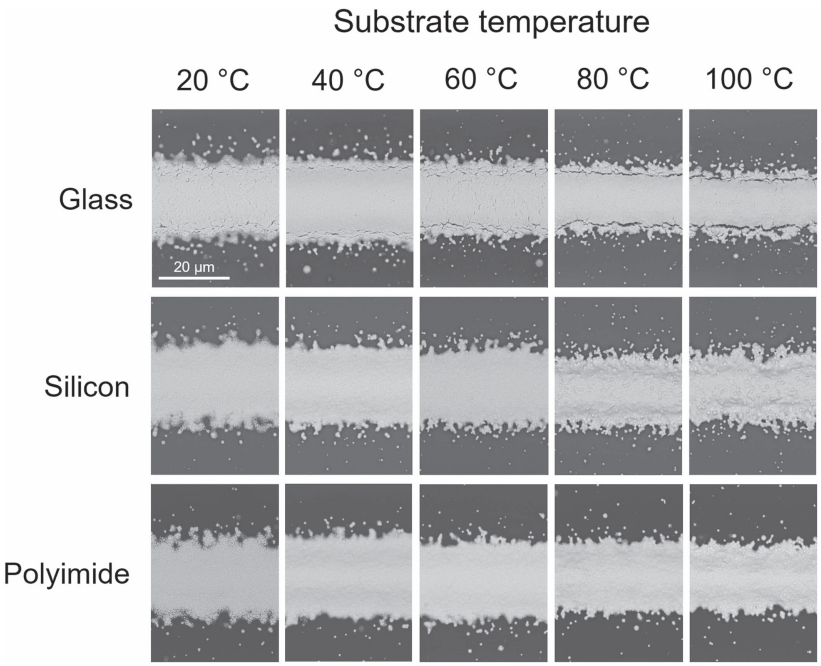

Figure 3. The influence of substrate temperature on aerosol jet printing of silver nanoparticle ink for three substrate materials; glass, silicon and polyimide. Line width appears to decrease with increasing substrate temperature, although overspray is more significant at higher temperatures. Through-thickness cracks are evident in lines printed onto glass at a high temperature.

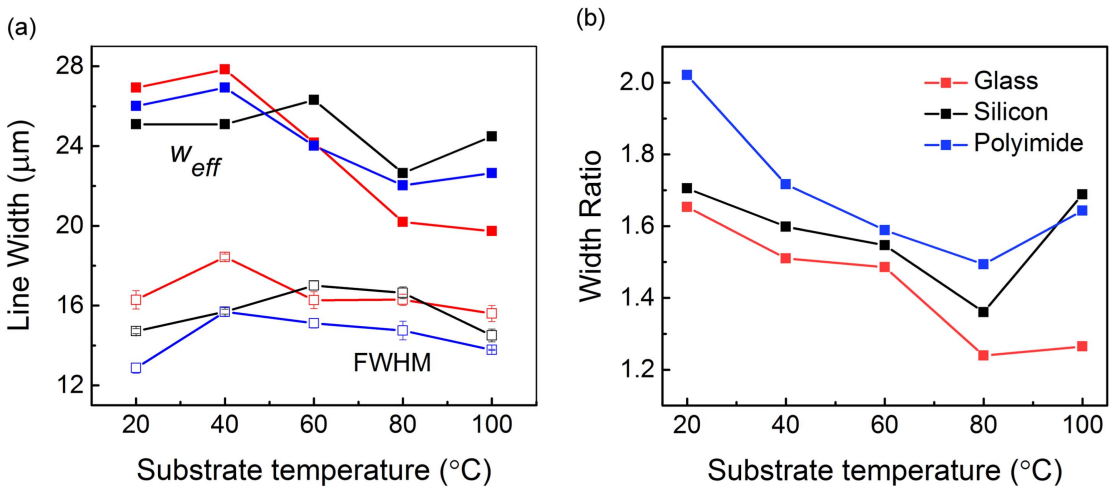

Figure 4. (a) The influence of substrate temperature and substrate material on the line width, measured using two different criteria. The ratio of the line widths is also shown. The error in each point is negligible in comparison to the size of the marker. (b) The width ratio—a metric for the quality of the printed line—decreases with increasing substrate temperature until the highest temperature studied, where temperature induced overspray becomes significant and broadens the line.

until 100 °C, where an increase is observed for all substrates as temperature induced overspray became significant. Correspondingly, the influence of substrate temperature on line resistivity is shown in figure 5. When cured for 1 h at 200 °C, none of the lines on silicon substrates were conducting, around two thirds of those on polyimide were conducting yet *all* of the lines printed on glass were conducting. Substrate temperature during printing was not found to be a reliable predictor for which samples cured successfully.

Curing for 2 h at 200 °C resulted in conducting lines on all substrates. On average the line resistivity was found to be between 3 and 4x that of bulk silver (also shown in figure 5 for comparison), which is comparable to that determined elsewhere [19]. The plot shows a tentative correlation between resistivity and substrate temperature. In general, a higher substrate temperature resulted in a more resistive line. For polyimide and silicon however, a slight dip in resistivity occurred at around 60 °C.

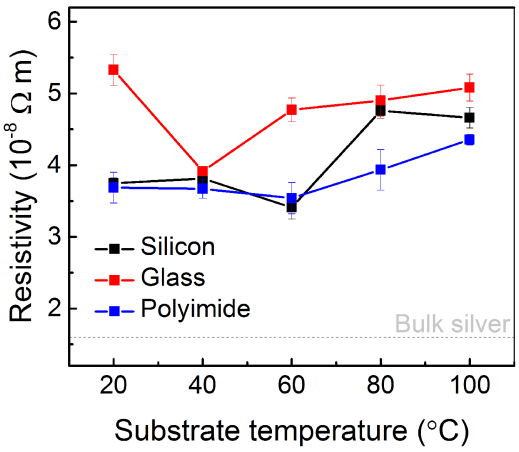

Figure 5. Variation in line resistivity as a function of substrate temperature. The resistivity of bulk silver is also shown for reference.

Figure 6 shows how the profile, area and resistivity of a line printed using identical parameters changed with time. The area steadily increased to almost four times the initial value after an hour of continuous printing. The variation in cross-sectional area also increased with print time. The resistivity of the lines was relativity constant throughout, however.

An example data set from a flex-test measurement is shown in figure 7(a), where resistance of a line printed on polyimide is plotted as a function of curvature of the substrate. The corresponding strain is also shown. The $R_0(\kappa)$ curve shows the resistance of the printed line while flat, immediately before it was deformed to curvature κ. This acts as a baseline measurement throughout the experiment, and is shown to gradually increase as the substrate is deformed to higher curvatures, reflecting the damage occurring to the printed line as a result of repeated bending. The resistance of the line whilst under deformation is displayed by the $R(\kappa)$ curve. This increased with curvature and is attributed to the elongation of the printed line along its length and lateral Poisson contraction of the current carrying area. At a curvature of around 300 m^{-1}, a large increase (~25%) in resistance occurred. The sample subsequently failed at the next curvature studied (~420 m^{-1}).

The ratio R/R_0 as a function of κ is shown in figure 7(b), along with the standard $(L/L_0)^2$ model for a conducting material under strain (albeit modified to accommodate curvature—derivation of this model is explained within the supplementary information). Shown in the figure are data from two different curing conditions. Both appear to be in reasonable agreement with the simple bending model. The large departure from the expected behaviour at the final curvature investigated before failure can be attributed to violations of the assumptions inherent in the simple model. Curing at a lower temperature for a longer period of time resulted in the line remaining conducting to a greater value of κ before failure.

4. Discussion

The influence of the focus ratio reported elsewhere has also been observed here [14, 15]. However, the quality of the printed line does not continue to improve indefinitely as the focus ratio is increased. The upper limit of focus ratio is set by a pressure limit which exists to prevent damage to the equipment. Before this limit is reached, however, the line quality is diminished by significant overspray. This occurs for all atomiser flow rates, but is most noticeable for atomiser flow rates above 25 sccm. It is likely that the high gas flow rates within the tip cause the flow to deviate from the normal laminar flow. Some turbulent mixing of sheath and atomiser flows may occur, causing a broadening of the deposition. The effects of other AJP-related parameters studied are discussed in detail below.

4.1. Influence of substrate temperature and material on line morphology

Overspray was found to become more significant on all substrate materials at higher substrate temperatures, as shown by the images in figure 3. This phenomenon, referred to here as 'temperature induced overspray' (to distinguish between overspray caused by deposition parameters) is likely to be due to the layer of air that becomes heated immediately above the substrate surface. The change in air density and possible convection currents may disrupt the aerosol jet and cause it to spread. The effect appears to be most significant when printing on silicon. This can be rationalised by considering that silicon has a significantly higher thermal conductivity than either glass or polyimide, meaning that the layer of air above the substrate is heated to a greater extent and thus has a greater influence on the aerosol jet. The substrate temperature was also found to have an effect on the printed line width, as discussed below in section 4.2.

Lines printed onto glass at temperatures greater than 40 °C were found to develop through-thickness cracks parallel to the line edge, however this is not seen on other substrates—see figures 3 and S3. The cracks may have been driven by differential thermal contraction upon cooling from the curing temperature. However, inspection of the coefficients of linear thermal expansion (CTE) (table 2) reveals that while there is a difference in CTE between silver (albeit taken as the bulk material) and glass, a greater difference exists between silver and silicon. If cracking is entirely caused by thermal contraction, then it should also be observed on silicon, which is not the case. Other factors must therefore be considered.

Adhesion between the ink and substrate material is likely to be another significant factor. The ink used in this study had relatively poor adhesion to glass, but

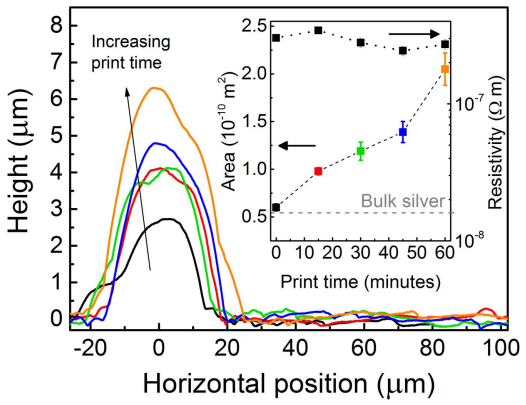

Figure 6. An illustration of system drift with respect to aerosol jet printing. The output of the system can be seen to increase over the period of an hour, with a four-fold increase in the cross-sectional line area. The resistivity, however, remains relatively constant.

showed good adhesion to silicon. Cracking therefore occurred in lines printed on glass, but not silicon, as the silver was able to de-bond from glass to release the thermal stress, while the greater bond between silver and silicon prevented spalling and likely resulted in some residual tensile stress. The fact that cracking becomes more evident for lines that are printed onto hotter substrates points again to the role of thermally generated stresses present in the process.

4.2. Influence of substrate temperature on line width and conductivity

Generally, a higher substrate temperature resulted in a narrower line width—a similar result to that observed by Kopola *et al* [20]. This is most easily seen in the FWHM criterion and can be understood by considering the rate of solvent evaporation and the reduced time for the deposited ink to spread. A general increase in the effective width at higher temperatures is attributed to temperature induced overspray, as discussed previously.

The reasons for the marginal *increase* in line width between 20 °C and 40 °C are not obvious. A possible explanation is the marginally higher substrate temperature acts to reduce the viscosity of liquid ink on the substrate surface, without significantly altering the rate of solvent evaporation. This allows the ink to spread further before the solvent dries. As the substrate temperature is increased further, solvent evaporation begins to dominate so any effects of reduced viscosity are negated.

The effects of substrate temperature on line width are best displayed using the width ratio. For each substrate material this is minimised at a temperature of 80 °C, i.e. these lines have the minimum amount of overspray per unit line width. The trend does not continue as temperature is increased further due to temperature induced overspray becoming significant, most notably on silicon, as previously discussed.

For applications in printed large area electronics, it is generally desirable to use the finest features possible to allow for a higher density of components whilst also minimising the amount of material required. However, this is only beneficial if achieving such a resolution does not reduce the line conductivity. Defining a quality factor (QF) as

$$\mathrm{QF} = \frac{\text{Conductivity of line}}{\text{Conductivity of bulk silver}} \times \frac{1}{\text{Width ratio}} \quad (2)$$

accounts for this limitation - effectively weighting the resolution of the line by its conductivity. An optimal line with minimal overspray and a conductivity comparable to that of bulk silver would have a quality factor approaching unity. Lines of poorer quality (i.e. lower resolution and/or lower conductivity) will result in lower values of the quality factor. This quality factor can be considered a figure of merit for printed electronics applications where both spatial resolution and line conductivity are important. All of the quantities involved are straightforward to measure, and a simple expression involving these is sufficient to illustrate how any given printing parameter affects the quality of the printed line.

In this instance, it can be seen from figure 8 that a maximum in quality factor occurs for both silicon and polyimide at a substrate temperature of 60 °C. Below this temperature, the greater line width causes a decrease in the quality factor due to the reduction in lateral resolution. At higher temperatures, marginally greater resistivity and, eventually, temperature induced overspray limit the conductivity and lateral resolution, also forcing a decrease in the quality factor. Lines printed onto glass substrates appear not to follow this trend, possibly related to issues with adhesion and cracking as discussed above. As with other deposition parameters, this result will likely be highly dependent on the particular ink and print system used, but in general this figure of merit approach can be used to determine an optimal range for a given deposition parameter.

4.3. Influence of curing conditions on the flexibility of printed silver lines

The $(L/L_0)^2$ model is often used for analysing conducting films under strain, most commonly for applications within *stretchable* electronics [21]. Using this model to analyse the characteristics of a printed line subject to *bending* is far less commonplace, despite the fundamental mechanics being equivalent. The work of Ahn *et al* presents some similar data, showing how the resistivity of a printed silver line varies with bend radius for both convex and concave curvatures [22]. The ability of the silver lines to stretch was also investigated for several different curing conditions. The work presented here demonstrates that these approaches can be combined to provide a rigorous analysis of flexible printed lines. This is made possible

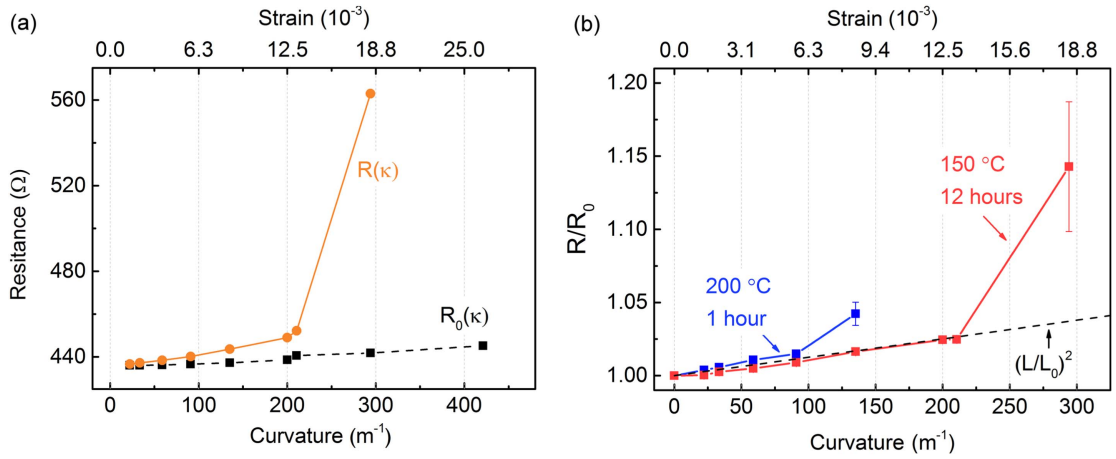

Figure 7. (a) An example data set from a flex test measurement. A large increase in resistance can be seen immediately before the sample fails. (b) The ratio of flat-to-flexed resistances is shown as a function of curvature for two different curing conditions. Both are in reasonable agreement with a simple analytical model for a conductor under strain due to bending. Curing at a lower temperature for longer time appears to improve the line flexibility.

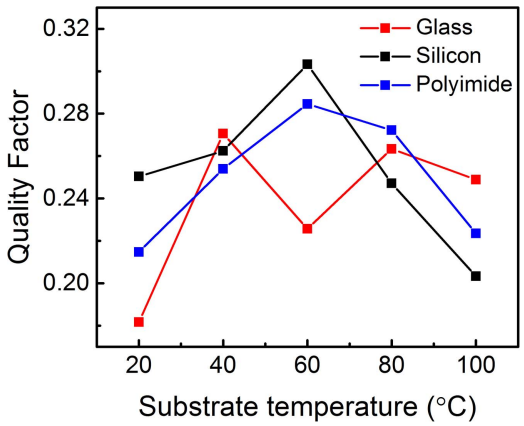

Figure 8. The variation of the quality factor figure of merit with substrate temperature. For silicon and polyimide, a maximum is evident at 60 °C, suggesting that this is a suitable temperature to use for applications this require well defined, narrow lines with reasonable conductivity.

Table 2. Coefficients of linear thermal expansion for the materials of interest [26].

Material	CTE (10^{-6} K^{-1})
Silver (bulk)	19.5
Glass	9
Polyimide	20
Silicon	3

by deforming the substrates to a *constant* curvature, rather than deforming into a sinusoid as is the case for a simply supported Euler strut.

Bulk silver is a relatively ductile metal, however the microstructure of a material formed from sintered Ag NPs is significantly more porous than that of the bulk, and therefore AJP printed Ag lines are not expected to be as ductile as the bulk material. The discrepancy in ductility between sintered and bulk silver is a well-known problem [23]. Nonetheless, the strains-at-failure observed in this work (a few percent strain) is consistent with that found elsewhere for silver NP inks [23, 24].

It was observed that the dominant failure mode of these silver lines was intergranular fracture. At a certain critical curvature (dependent on the curing conditions), the density of these cracks was sufficient to dramatically reduce the number of conducting paths along the line, leading to a dramatic increase in the line resistance. Such behaviour could be interpreted as a 'percolation threshold' of cracks. Low temperature curing generally leads to a smaller grain size than higher temperature curing [25]. With larger grains, it is far more likely that these cracks will propagate through the thickness of the line, thus creating a break in the line and causing the sample to fail. Hence, curing at a higher temperature reduces the line flexibility. The large variation in resistance at the final curvature tested before failure reflects the stochastic nature of the crack-driven failure mechanism.

However, while the fine grain structure of low temperature cured lines did appear to improve their flexibility (see figure 7(b)), the resistivity (not shown) was around 4–5 times larger than those cured at 200 °C (~20x bulk, compared to ~4x bulk, respectively), so a compromise between flexibility and conductivity must be reached. It is possible that the relationship between flexibility and curing temperature does not continue indefinitely, and that inks cured at high temperatures may approach the ductility of bulk silver as the porosity of the deposition is reduced. It should be noted that neither the ink used nor the printed pattern were formulated to optimise flexibility. It is conceivable that some other pattern design might lead to improved flexibility purely due to

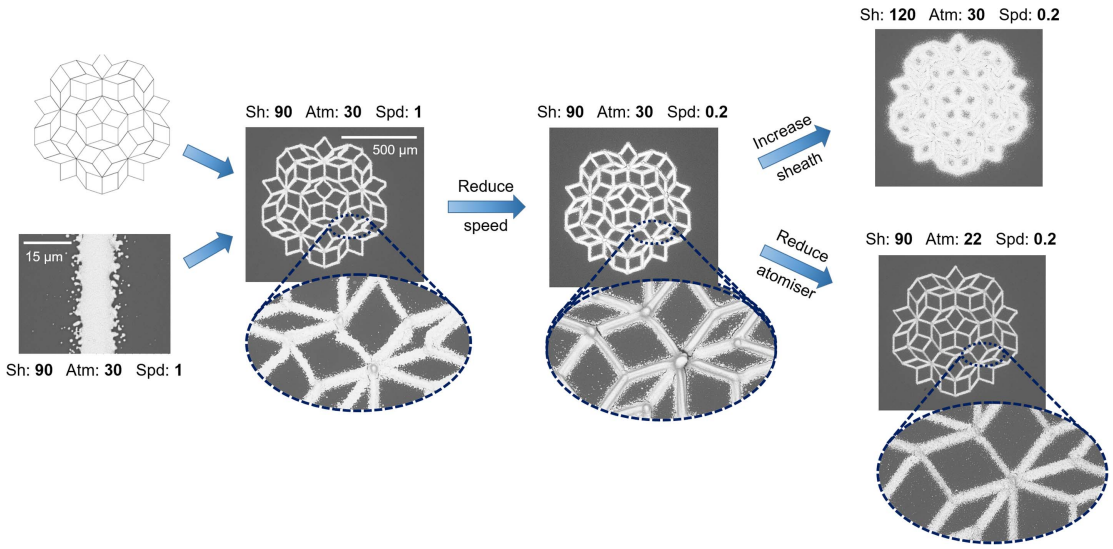

Figure 9. An example of how deposition can be improved subject to constraints imposed by a particular application. In this instance, a low print speed is required to ensure accurate platen motion. To mitigate the effects this has on the line morphology, the focus ratio can be increased—importantly, this is achieved by *reducing* the atomiser flow rate, rather than increasing the sheath flow.

its geometry. The fine scale deposition that AJP is capable of ought to allow such patterns to be produced.

4.4. System drift

An important issue that has not been previously discussed with respect to AJP is that of system *drift*. This describes the change in printed line morphology over time, despite the same deposition parameters being used. This means that any empirical or theoretical relationship that correlates a set of deposition parameters to a line morphology must also account for the entire print history. The exact characteristics of this phenomenon are likely to be highly dependent on the individual print system and ink used. For the system used in this particular study, it was observed that the amount of material deposited per unit time would increase over the duration of a print, as shown in figure 6.

Given that the increase in line area is roughly linear in time, the effect of this drift on large individual samples could be minimised by reversing the direction of print for alternate layers. The system can be 'reset' by cleaning the entire atomiser assembly, suggesting that drift in this case is caused by the accumulation of liquid ink within the atomiser components. It is possible that as the atomiser gas flow passes through these contaminated components, some of the accumulated ink is entrained within the flow, thus increasing the ink loading and resulting in greater deposition. If the exact deposition parameters are unimportant (i.e. only a conducting line is needed, no correlation is sought between deposition parameters and line morphology) then the atomiser flow rate can be reduced periodically in time, with appropriate sheath adjustments, to ensure that the print remains stable.

4.5. Framework for controlling the morphology of printed lines

The parameter space for the AJP process is large and extensively interrelated, but nonetheless the work of Goth [13], Mahajan [14] and Binder [15] *et al* is very useful in identifying some overall trends. The number of parameters that can be changed means that determining a set of universal 'optimal' deposition parameters is non-trivial: a given line morphology could be achieved using several different sets of deposition parameters—as shown by some of the results presented by Kopola *et al* [20].

The exact set of parameters that should be used will be dictated by the particular demands of the application. As an example, consider the pattern of Penrose tiles shown in figure 9. One might wish to replicate the morphology of the single line shown for use with this pattern. However, simply applying the same print parameters is unsuccessful, as the first image shows. Instabilities in the platen motion at small scales and relatively high print speeds cause distortions to the straight lines. Slowing the print speed down allows for more accurate platen motion, however now the line morphology is changed significantly to a wider, taller line. To counteract this, the focus ratio can be increased. This can be achieved either by reducing the atomiser flow or increasing the sheath flow. Both of these options are shown in figure 9, and while both depositions used approximately the same focus ratio, the results are markedly different. The optimal approach is to reduce the atomiser flow rate such that the amount of material deposited per unit distance is broadly unchanged from the initial line which we are attempting to reproduce.

While these points have been eluded to by Mahajan *et al* they have been presented here in the context of

how a user may arrive at a set of acceptable deposition parameters for a given application. The main point of this discussion is that whilst focus ratio is a useful parameter, many other factors must also be considered when determining an appropriate set of deposition parameters.

5. Conclusions

An optimum operation window was first determined for aerosol jet printed silver lines based on atomiser gas flow rate and focus ratio. Following this, the influence of substrate temperature on the line morphology was studied for three substrate materials: silicon, glass and polyimide. The results showed that the morphology of lines printed onto a low temperature substrate are broadly independent of substrate material. As the substrate temperature is increased, differences between the materials become apparent. By comparing the line widths obtained using two different criteria, namely a microscopy based 'effective' width and a profilometry based FWHM, it was demonstrated that temperature induced overspray becomes a significant issue on silicon substrates at high temperatures. This is thought to be due to the layer of heated air above the substrate surface. Cracking of lines printed onto glass substrates occurs at a high temperature. It is believed this is due to differential thermal contraction, although the exact cause, and why it only affects glass and no other substrate materials, is not completely understood. The resistivity of printed lines increases slightly with substrate temperature. The conclusion (for this particular ink and print system) is that for an application that requires narrow, well-defined lines with reasonable conductivity, a substrate temperature of around 60 °C–80 °C would be most suitable. The issue of system drift, whereby the deposition changes over time, has also been discussed. It was found that the printer output increased over time, resulting in taller and wider lines. Some mitigating strategies were developed to minimise the influence of this.

The flexibility of silver lines printed on polyimide substrates was also assessed. A model was developed to demonstrate how the mechanics of flexible electronics can be characterised. It was shown that curing at lower temperatures for longer times can improve the flexibility of Ag NP ink, albeit at the expense of marginally reduced conductivity. Finally, a framework for arriving at an acceptable set of deposition parameters has been proposed. This highlights the fact that the choice of parameters is strongly dependent on the exact application, since some aspects of the deposition, perhaps print speed or substrate temperature, may be constrained. These limitations must be considered when determining an optimal operational window. It is hoped that by studying the characteristics of aerosol jet printing, a greater understanding of the process can be achieved allowing for further progress and innovation in the field of wide area and flexible electronics.

Acknowledgments

SK-N, MS and YSC are grateful for financial support from the European Research Council through an ERC Starting Grant (Grant No. ERC-2014-STG-639526, NANOGEN). MS and YSC acknowledge studentship funding from the Cambridge Commonwealth, European & International Trust. CB thanks the EPSRC Cambridge NanoDTC, EP/G037221/1, for studentship funding. Supporting data for this paper is available at the DSpace@Cambridge data repository (https://doi.org/10.17863/CAM.7286).

References

[1] Huang S H, Liu P, Mokasdar A and Hou L 2013 Additive manufacturing and its societal impact: a literature review *Int. J. Adv. Manuf. Technol.* **67** 1191–203
[2] O'Donnell J, Kim M and Yoon H-S 2016 A review on electromechanical devices fabricated by additive manufacturing *J. Manuf. Sci. Eng.* **139** 10801
[3] Tan E, Jing Q, Smith M, Kar-Narayan S and Occhipinti L 2017 Needs and enabling technologies for stretchable electronics commercialization *MRS Adv.* 1–9
[4] Castrejon-Pita J and Baxter W 2013 Future, opportunities and challenges of inkjet technologies *At. Sprays.* **23** 1–13
[5] Seifert T, Sowade E, Roscher F, Wiemer M, Gessner T and Baumann R R 2015 Additive manufacturing technologies compared: morphology of deposits of silver ink using inkjet and aerosol jet printing *Ind. Eng. Chem. Res.* **54** 769–79
[6] Hoath S, Martin G D and Hutchings I M 2010 Effects of fluid viscosity on drop-on-demand ink-jet break-off *NIP26 Digit. Fabr. 2010* pp 10–3 (http://citeseerx.ist.psu.edu/viewdoc/summary?)
[7] Maiwald M, Werner C, Zoellmer V and Busse M 2010 INKtelligent printed strain gauges *Sensors Actuators* A **162** 198–201
[8] Cho J H, Lee J, Xia Y, Kim B, He Y, Renn M J, Lodge T P and Daniel Frisbie C 2008 Printable ion-gel gate dielectrics for low-voltage polymer thin-film transistors on plastic *Nat. Mater.* **7** 900–6
[9] Grunwald I, Groth E, Wirth I, Schumacher J, Maiwald M, Zoellmer V and Busse M 2010 Surface biofunctionalization and production of miniaturized sensor structures using aerosol printing technologies *Biofabrication* **2** 14106
[10] Marquez G J, Renn M J and Miller W D 2002 Aerosol-based direct-write of biological materials for biomedical applications *Electroact. Polym. Rapid Prototyp.* **698** 343–9
[11] Ha M, Seo J-W T, Prabhumirashi P L, Zhang W, Geier M L, Renn M J, Kim C H, Hersam M C and Frisbie C D 2013 Aerosol jet printed, low voltage, electrolyte gated carbon nanotube ring oscillators with sub-5 μs stage delays *Nano Lett.* **13** 954–60
[12] Tait J G, Witkowska E, Hirade M, Ke T H, Malinowski P E, Steudel S, Adachi C and Heremans P 2015 Uniform aerosol Jet printed polymer lines with 30 μm width for 140 ppi resolution RGB organic light emitting diodes *Org. Electron. Phys. Mater. Appl.* **22** 40–3
[13] Goth C, Putzo S and Franke J 2011 Aerosol Jet printing on rapid prototyping materials for fine pitch electronic applications *2011 IEEE 61st Electronic Components and Technology Conf.* (Piscataway, NJ: IEEE) pp 1211–6
[14] Mahajan A, Frisbie C D and Francis L F 2013 Optimization of aerosol jet printing for high-resolution, high-aspect ratio silver lines *ACS Appl. Mater. Interfaces.* **5** 4856–64
[15] Binder S, Glatthaar M and Rädlein E 2014 Analytical investigation of aerosol jet printing *Aerosol Sci. Technol.* **48** 924–9

[16] Folgar C E, Suchicital C and Priya S 2011 Solution-based aerosol deposition process for synthesis of multilayer structures *Mater. Lett.* **65** 1302–7
[17] Mahajan A, Francis L F and Frisbie C D 2014 Facile method for fabricating flexible substrates with embedded, printed silver lines *ACS Appl. Mater. Interfaces.* **6** 1306–12
[18] Jabari E and Toyserkani E 2016 Aerosol-jet printing of highly flexible and conductive graphene/silver patterns *Mater. Lett.* **174** 40–3
[19] Hoey J M, Lutfurakhmanov A, Schulz D L and Akhatov I S 2012 A review on aerosol-based direct-write and its applications for microelectronics *J. Nanotechnol.* **2012** 1–22
[20] Kopola P, Zimmermann B, Filipovic A, Schleiermacher H F, Greulich J, Rousu S, Hast J, Myllylä R and Würfel U 2012 Aerosol jet printed grid for ITO-free inverted organic solar cells *Sol. Energy Mater. Sol. Cells* **107** 252–8
[21] Glushko O and Cordill M J 2014 Electrical resistance of metal films on polymer substrates under tension *Exp. Tech.* **40** 9–12
[22] Ahn B Y, Duoss E B, Motala M J, Guo X, Park S-I, Xiong Y, Yoon J, Nuzzo R G, Rogers J A and Lewis J A 2009 Omnidirectional printing of flexible, stretchable, and spanning silver microelectrodes *Science* **323** 1590–3
[23] Sim G-D, Won S and Lee S-B 2012 Tensile and fatigue behaviors of printed Ag thin films on flexible substrates *Appl. Phys. Lett.* **101** 191907
[24] Kim S, Won S, Sim G-D, Park I and Lee S-B 2013 Tensile characteristics of metal nanoparticle films on flexible polymer substrates for printed electronics applications *Nanotechnology* **24** 85701
[25] Kim I, Song Y A, Jung H C, Joung J W, Ryu S and Kim J 2008 Effect of microstructural development on mechanical and electrical properties of inkjet-printed ag films *J. Electron. Mater.* **37** 1863–8
[26] Engineering Toolbox, Coefficients of Linear Thermal Expansion, (n.d.). http://engineeringtoolbox.com/linear-expansion-coefficients-d_95.html (accessed 2 November 2016)